

Increased exposure to pollutant aerosols under high voltage power lines

A. P. FEWS, D. L. HENSHAW*, P. A. KEITCH, J. J. CLOSE and R. J. WILDING

(Received 23 April 1999; accepted 8 August 1999)

Abstract.

Purpose: To assess increased exposure to airborne pollutants near power lines by investigating theoretically and experimentally the behaviour of ^{222}Rn decay product marker aerosols in the 50 Hz electric field under power lines.

Materials and methods: The behaviour of aerosols in outdoor air including those carrying ^{222}Rn decay products was modelled theoretically in the presence of an AC field. TASTRAK α -particle spectroscopy was used to characterize ^{218}Po and ^{214}Po aerosols outdoors. Sampling points were chosen along a line at right angles up to 200 m from a number of high voltage power (transmission) lines. Each sampling point comprised an arrangement of mutually orthogonal TASTRAK detectors. Exposures were carried out at different power line locations in various weather conditions.

Results: The model predicts a two- to three-fold increase in deposition of aerosols on spherical surfaces mimicking the human head under high voltage power lines. Experimental measurements using detectors mounted on grounded metal spheres showed an enhanced deposition of both ^{218}Po and ^{214}Po aerosols. Enhanced ^{218}Po deposition on 400 kV lines ranged from 1.96 ± 0.15 to 2.86 ± 0.32 . Enhanced ^{214}Po deposition on 275 kV and 132 kV lines were 1.43 ± 0.07 and 1.11 ± 0.21 , respectively, where the latter value was not significant.

Conclusions: The observations demonstrate a mode of increased exposure to pollutant aerosols under high voltage power lines by increased deposition on the body. The total (indoor + outdoor) ^{218}Po and ^{214}Po dose to the basal layer of facial skin is estimated to be increased by between 1.2 and 2.0 for 10% of time spent outdoors under high voltage power lines.

1. Introduction

Epidemiological studies have demonstrated an association between exposure to power frequency electromagnetic fields (EMF) and increased incidence of childhood leukaemia. The associations are strongest for exposures under high voltage power lines (Ahlbom *et al.* 1993, Feychting and Ahlbom 1993, Olsen *et al.* 1993, Verkasalo *et al.* 1993, NRPB 1994, NIEHS 1998). No causal mechanism to explain these associations has yet been convincingly identified. However, on the strength of the epidemiological data, the US National Institute of Environmental Sciences Working Group has recently stated that

electric and magnetic fields like those surrounding electric power lines should be regarded as a possible human carcinogen (NIEHS 1998), and the full report to the US Congress recommends that the power industry continue its current US practice of siting power lines to reduce exposures (NIEHS 1999).

The search for a causal mechanism by which exposure to power frequency EMF may affect the process of carcinogenesis has tended to concentrate on direct effects from the magnetic field component. The authors are, however, studying a number of ways in which the electric, E-field component interacts with airborne pollutant aerosols, each suggesting a mechanism of increased exposure to these pollutants under high voltage power lines. The relevance of this approach is that both childhood and adult leukaemia are known to be associated with traffic density and its associated exhaust pollution (Savitz and Feingold 1989, Lindquist *et al.* 1991, Robinson 1991, Nordlinder and Järholm 1997).

Henshaw *et al.* (1996) described two possible mechanisms of increased exposure to pollutants near power frequency E-field sources. In indoor experiments using ^{222}Rn decay product marker aerosols, an excess deposition of these aerosols on surfaces carrying a power frequency electric potential and an increased concentration in air near the electric field source were observed.

Excess deposition of ^{222}Rn decay product marker aerosols on surfaces mimicking the human head has now been observed outdoors under 400, 275 and 132 kV high voltage overhead transmission lines (here referred to as power lines). Results of these deposition measurements are reported in this paper.

2. Materials and methods

2.1. Theoretical modelling

2.1.1. *Theoretical analysis of atmospheric ^{222}Rn decay product aerosols in AC fields.* The processes that govern the production and loss of aerosols in outdoor air have been summarized by Hinds (1982). Positive or negative ions present in the air act as nucleation sites,

*Author for correspondence.

H. H. Wills Physics Laboratory, University of Bristol, Tyndall Avenue, Bristol BS8 1TL, UK.

which attract polar molecules forming a cluster of molecules 1–4 nm in diameter. Such a molecular cluster constitutes a so-called ultrafine aerosol. The high diffusivity of these aerosols $(4\text{--}9) \times 10^{-6} \text{ m}^2 \text{ s}^{-1}$ results in frequent collisions, leading to rapid growth by coagulation up to $\sim 0.1 \mu\text{m}$ in size. The diffusivity of these larger aerosols is around four orders of magnitude lower: $\sim 2 \times 10^{-10} \text{ m}^2 \text{ s}^{-1}$.

The experimental measurements described below employ ^{222}Rn decay product aerosols as markers of general aerosol behaviour. The principle of this marker is the different behaviour in air of the ultrafine and aerosol-attached ^{222}Rn decay products (Porstendörfer 1984, 1994, Raes 1985). The attachment rate in outdoor air of ultrafine particles to the ambient aerosol is typically in the range $30\text{--}100 \text{ h}^{-1}$.

The growth of ^{222}Rn decay product aerosols is shown schematically in figure 1. A key feature is that 90% of recoil ^{218}Po from ^{222}Rn is positively charged allowing the rapid nucleation of an ultrafine aerosol as described above (see Hopke 1989 and references therein). A similar ^{214}Pb recoil occurs following the decay of ^{218}Po , resulting in a 0.8 probability of detachment from an attached aerosol (Mercer 1976). This process, however, is not repeated for the subsequent β -decays due to the low recoil energy. Two other features should be noted. As explained below, the present authors are interested in detecting the deposition of these aerosols by recording α -emission from ^{218}Po and ^{214}Po using α -sensitive TASTRAK plastic track detectors (based on poly allyl diglycol carbonate plastic; supplied by Track Analysis Systems Ltd, H. H. Willis Physics Laboratory, Briston, UK). The mean lifetime of ^{218}Po is 4.4 min, so that in the absence of other loss mechanisms, the above rate of aerosol attachment suggests that between 14% and 48% of ^{218}Po in air is in ultrafine form. The majority (95–99%) of ^{218}Po deposition recorded on TASTRAK detectors will be from ultrafine aerosols due to their high diffusivity. Conversely, the combined lifetimes of the aerosols feeding the subsequent ^{214}Po decay is sufficiently large that essentially all ^{214}Po decays in air are in attached form. However, those ^{214}Po deposition decays recorded on TASTRAK result from earlier deposition, which may be in either ultrafine or attached aerosol form.

The present work was aimed at measuring excess deposition of aerosols under power lines, and in modelling the expected increased deposition on spherical surfaces, similar to that which occurs around the human head. In AC fields the excess deposition occurs by the oscillation, coupled with turbulent diffusion, of charged aerosol particles along the E-field line vectors. The drift velocity v (m s^{-1}) of a charged aerosol in an E-field of strength E (V m^{-1}) is given

by $v = \mu E$, where μ is the particle mobility, typically $1.5 \times 10^{-4} \text{ m}^2 \text{ s}^{-1} \text{ V}^{-1}$ (Tyndall 1938).

Of crucial importance to the transport of ^{218}Po in E-fields is the recoil charge neutralization time (nominally $\sim 1 \text{ s}$ in figure 1). This has been investigated by several authors in laboratory measurements (Hopke 1989, Shi and Hopke 1991, Howard and Strange 1992). The published data, however, do not readily extrapolate to conditions outdoors so that there is uncertainty in the actual neutralization time.

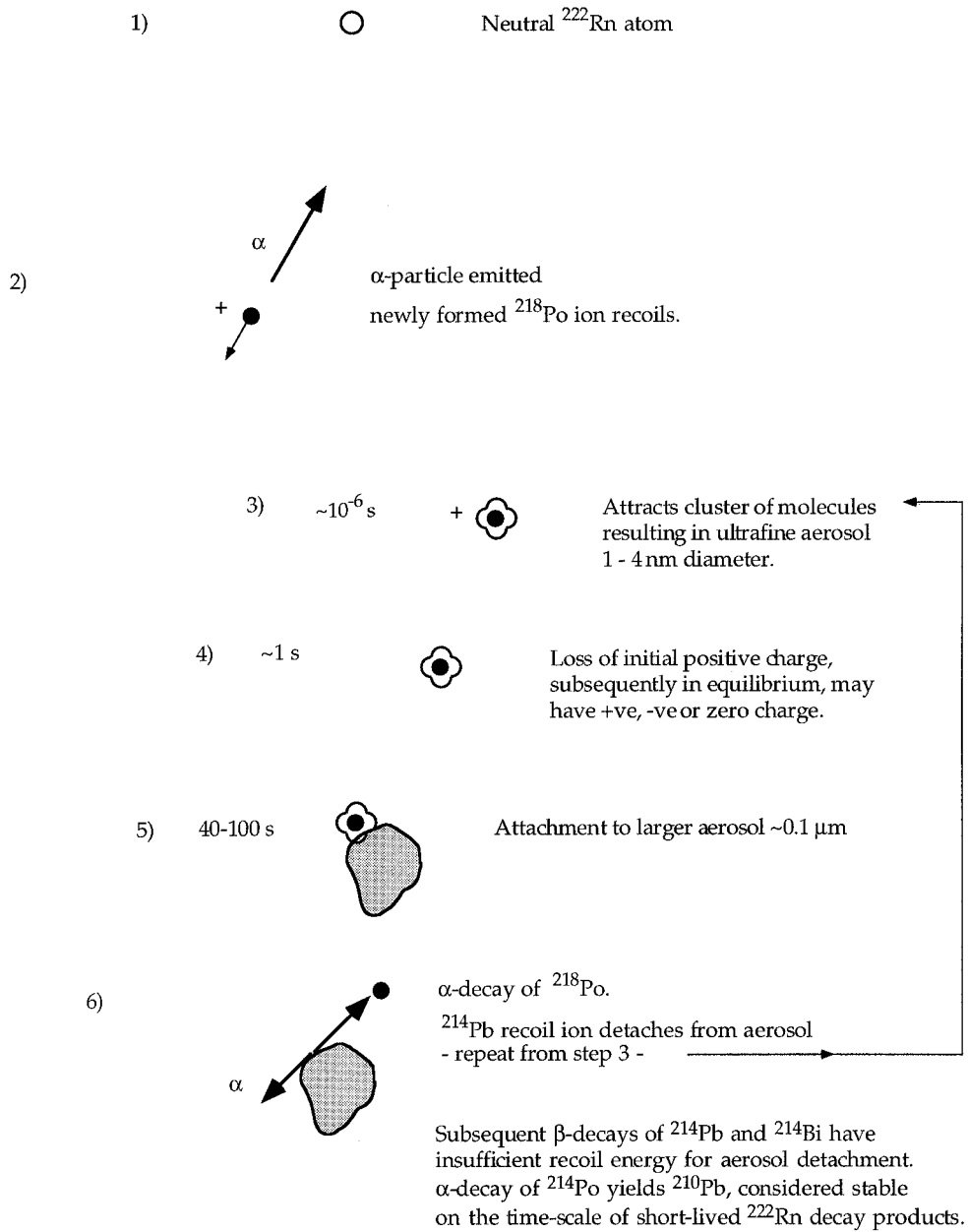
Under high voltage power lines the maximum recommended E-field is 10 kV m^{-1} (ICNIRP 1998). In practice such E-fields are usually in the range $1\text{--}6 \text{ kV m}^{-1}$. Because the human body is a good conductor, the field will be enhanced by a factor of approximately 18 around the head.

2.1.2. Description of an aerosol transport model in AC fields.

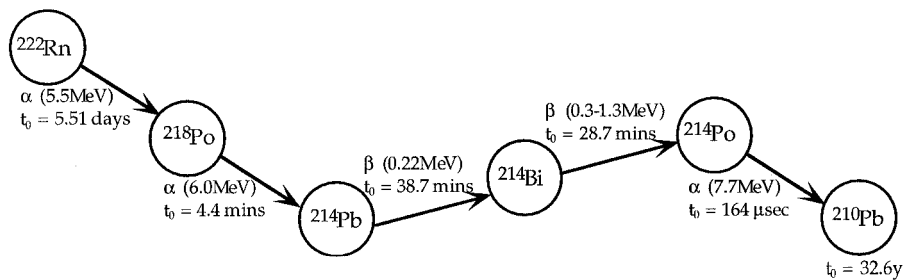
Aerosol transport in the atmosphere and surface deposition is modelled using a one dimensional algorithm. Figure 2 summarizes the transport pathways. ^{214}Po is not shown because of its short half-life. It is assumed to decay instantaneously following the decay of ^{214}Bi . The various constants are defined below. The model divides the atmosphere into n cells vertically. The first cell accommodates the source term for ^{222}Rn , which emanates from the ground, and the deposition onto the ground of the decay product aerosols. The remaining cells are identical with the n th cell coupled to neighbouring cells by atmospheric diffusion and the following quantities: (1) oscillation in the AC field; (2) the drift in the Earth's natural DC field; (3) gravitational settling; and (4) the deposition under the action of the mirror charge close to a surface. The aerosol-attached particles are assumed to have a Boltzmann charge distribution. Typically, 100 cells are used, the sizes of which increase exponentially from an initial size of 10^{-8} m in the first cell. The model treats radioactive decay and includes the aerosol attachment rates.

The pathways within a given cell can be described by a series of steady state equations, which can be solved for the activity concentration of the surface deposited ^{218}Po and ^{214}Po aerosols. These measurable quantities allow the model to be tested experimentally. The following are employed as standard values:

$$\begin{aligned} \lambda_{\text{Rn}} &= ^{222}\text{Rn decay constant} = 2.111 \times 10^{-6} \text{ s}^{-1} \\ \lambda_{\text{Po}} &= ^{218}\text{Po decay constant} = 3.787 \times 10^{-3} \text{ s}^{-1} \\ \lambda_{\text{Pb}} &= ^{214}\text{Pb decay constant} = 4.31 \times 10^{-4} \text{ s}^{-1} \\ \lambda_{\text{Bi}} &= ^{214}\text{Bi decay constant} = 5.86 \times 10^{-4} \text{ s}^{-1} \\ \lambda_{\text{a}} &= \text{attachment rate of ultrafine aerosols to} \\ &\quad \text{larger aerosols} = 0.01 \text{ s}^{-1} \text{ for a } 200 \text{ nm} \\ &\quad \text{aerosol at a nominal aerosol density of} \\ &\quad 7000 \text{ cm}^{-3} \text{ (Porstendörfer 1994)} \end{aligned}$$



(a)



(b)

Figure 1. (a) Growth of ^{222}Rn decay product aerosols; (b) ^{222}Rn short-lived radionuclide decay chain.

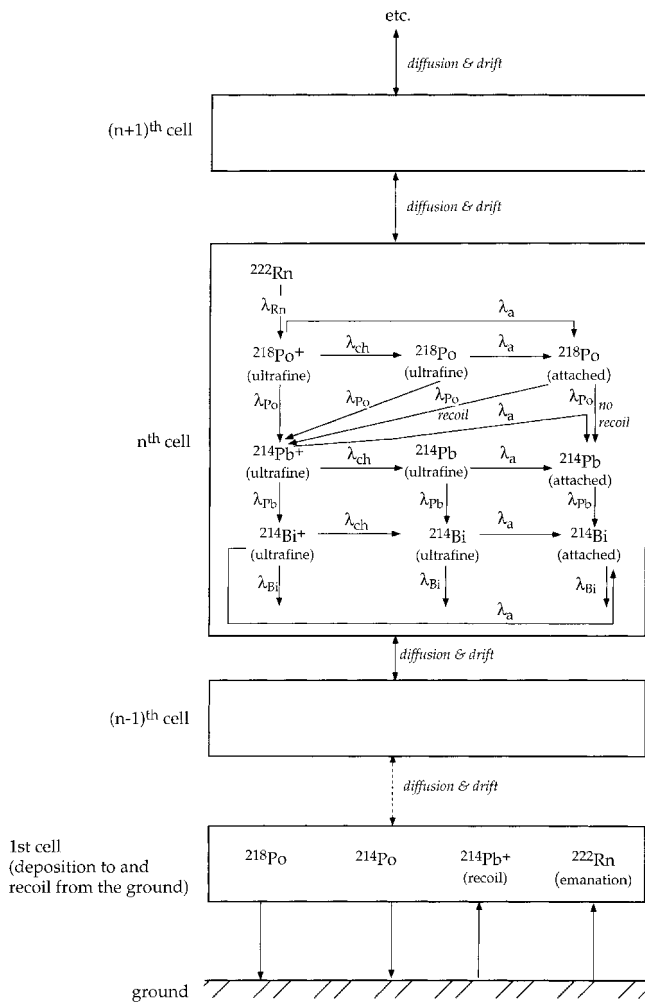


Figure 2. Schematic outline of the pathways used to model the behaviour of ^{222}Rn decay product aerosols in the atmosphere. The particle drift is made up of contributions from gravity, the Earth's natural DC field and the AC field.

λ_{ch} = rate constant for neutralization of the charged ultrafine ions = 2 s^{-1}

X_{218} = re-suspension source term (in $\text{Bq m}^{-3} \text{ s}^{-1}$) of ^{214}Pb from decay and recoil of deposited ^{218}Po , into $50 \mu\text{m}$ air layer (Jacobi 1972).

These ^{214}Pb recoil particles are distributed uniformly with distance over the cells that are within the recoil range.

r_a = recoil fraction of ^{214}Po in air = 0.8 (Mercer 1976)

r_p = recoil fraction of ^{214}Po following decay of plated-out ^{218}Po = 0.5

Earth's DC field = 100 V m^{-1}

Gravity is assumed active unless otherwise stated.

The general transport equation for species j in

spherical geometry with distance r and time t is given by:

$$\frac{\partial C_j(r, t)}{\partial t} = \frac{1}{r^2} \frac{\partial}{\partial r} \left[\left((D_{jB} + D_T(r)) \frac{\partial C_j(r, t)}{\partial r} - V_j(r, t) \cdot C_j(r, t) \right) r^2 \right] - \lambda_j C_j(r, t) + S_j(r, t) \quad (1)$$

where C_j is the concentration of species j , and S_j is a species-dependent additional term representing the pathways shown in figure 2 as follows:

$$\begin{aligned} S_1 &= 0 && (^{222}\text{Rn atoms}) \\ S_2(r, t) &= \lambda_1 C_1(r, t) - (\lambda_{\text{ch}} + \lambda_a) C_2(r, t) && (\text{charged ultrafine } ^{218}\text{Po ions}) \\ S_3(r, t) &= \lambda_{\text{ch}} C_2(r, t) - \lambda_a C_3(r, t) && (\text{neutral ultrafine } ^{218}\text{Po atoms}) \\ S_4(r, t) &= \lambda_a [C_2(r, t) + C_3(r, t)] && (\text{aerosol-attached } ^{218}\text{Po atoms}) \\ S_5(r, t) &= \lambda_2 C_2(r, t) + \lambda_3 C_3(r, t) - (\lambda_{\text{ch}} + \lambda_a) C_5(r, t) \\ &\quad + \lambda_4 \cdot r_a \cdot C_4(r, t) + r_p \cdot X_{218} && (\text{charged ultrafine } ^{214}\text{Pb ions}) \\ S_6(r, t) &= \lambda_{\text{ch}} C_5(r, t) - \lambda_a C_6(r, t) && (\text{neutral ultrafine } ^{214}\text{Pb atoms}) \\ S_7(r, t) &= \lambda_a [C_5(r, t) + C_6(r, t)] + \lambda_4 (1 - r_a) C_4(r, t) && (\text{aerosol-attached } ^{214}\text{Pb atoms}) \\ S_8(r, t) &= \lambda_a [C_5(r, t) + C_6(r, t)] + \lambda_4 (1 - r_a) C_4(r, t) && (\text{charged ultrafine } ^{214}\text{Bi ions}) \\ S_9(r, t) &= \lambda_a [C_5(r, t) + C_6(r, t)] + \lambda_4 (1 - r_a) C_4(r, t) && (\text{neutral ultrafine } ^{214}\text{Bi ions}) \\ S_{10}(r, t) &= \lambda_a [C_5(r, t) + C_6(r, t)] + \lambda_4 (1 - r_a) C_4(r, t). && (\text{aerosol-attached } ^{214}\text{Bi atoms}) \end{aligned}$$

V_j = drift velocity of species j due to E-fields and gravity

n_j = number of charges on species j particles

K_1 = atmospheric diffusion constant

K_2 = diffusion constant near deposition surface

The Brownian diffusion and the particle drift velocity are as follows:

$$D_{jB} = \mu_j \cdot \frac{kT}{e} \quad (2)$$

$$V_j = -n_j \cdot \mu_j \cdot \left[\frac{mg}{e} + E_{\text{DC}} + \sqrt{2} \cdot E_{\text{rms}}(r) \cdot \sin(2\pi 50t) \right] \quad (3)$$

where e is the electronic charge, k the Boltzmann's constant and T the absolute temperature. In a 50 Hz E-field, the aerosol will oscillate with a peak-to-peak amplitude of $(\sqrt{2} \mu E_{\text{rms}}) / (50\pi)$. $E(r)$ has the variation with distance $E(r) = E_0 / r^2$, and gravity is assumed to be invariant with distance. At the boundary where

$r=0$, C_j will fall to zero. The aerosol-attached ^{218}Po and ^{214}Po are assumed to have a Boltzmann distribution of charge, which has been found to be a good empirical description of the charge state for particles of 200 nm diameter being modelled here (Hinds 1982). It is possible that the attached ^{214}Pb and ^{214}Bi might have an excess positive charge from the earlier radioactive decays (Clement and Harrison 1992). Any initial excess charge will tend to increase the enhanced (E-field) deposition. However, the model does not allow for this because we consider that neutralization by ambient air ions will generally be fast enough to ensure that the charge distributions are close to the Boltzmann distribution. Because each charge state will drift differently in E-fields, equations for C_4 , C_7 and C_{10} are themselves subdivided into five components, representing the five most probable charge states. Each component is treated separately for diffusion and drift and then recombined to give the total concentration of attached ^{218}Po and ^{214}Po . This system of linked equations is written in a finite difference form and solved sequentially by the Crank–Nicholson algorithm.

The mobility of ultrafine aerosols is taken as $1.5 \times 10^{-4} \text{ m}^2 \text{ V}^{-1} \text{ s}^{-1}$, the average of reported values. The attached aerosols have an assumed diameter of 200 nm, leading to a mobility of $8.3 \times 10^{-9} \text{ m}^2 \text{ V}^{-1} \text{ s}^{-1}$, using the data of Cheng *et al.* (1992). The calculation can use either an exact treatment for particle motion where all the charged particles oscillate with the AC phase, or the dividing surface approximation similar to that used by Mayya and Sapra (1997). The latter is used (e.g. for indoor simulation) where it is a good approximation. For outdoor conditions of high deposition velocity (and short turbulence time scales compared with the AC period), this approximation is poor and the exact method is used instead.

2.1.3. *Model parameters.* The calculation is run in two stages. The first sets up the vertical concentration profile of the particles, by including transport to the open atmosphere. The second estimates the deposition on the test surface (here a 20 cm diameter sphere represents the human head) at a specified height by using the calculated profile from the first stage and letting turbulent diffusion transport these particles to the surface. This allows a perturbed E-field deposition to be calculated, which will locally affect deposition but will not change the overall atmospheric profile.

The first stage simply seeds the main calculation with appropriate particle concentrations giving reasonable values of F and f (radon decay product equilibrium fraction and ultrafine fraction), by using

a simple form for the turbulent diffusion away from the ground, $D_T = K_1 r$. This linear form is similar to that used by Porstendörfer (1994) and Jacobi and André (1963), and can represent a form of flow-induced turbulence studied by Sehmel (1973). Values of the constant K_1 between 10^{-3} and 1 were tested to represent different weather conditions, but were found to have a negligible effect on the deposition, which was determined as discussed below by the form of turbulent diffusion close to the test surface. In other words, uncertainty in atmospheric transport has little effect on deposition close to the ground, and only the diffusion coefficient close to the ground is relevant. Note that this is almost irrelevant for ^{218}Po deposition because this is determined almost totally from the ultrafine particle deposition.

Deposition close to the test surface was modelled using different forms of D_T , in order to overcome the uncertainty of which form to use. Thus, the form $D_T = K_2 r^n$ was used, with $n = 1.5, 2.0$ and 3.0 . The quadratic form is the same as that used by Crump and Seinfeld (1981) and Mayya and Sapra (1997). This form enables the simulation to reproduce the experimental observation by Porstendörfer (1994) that the ultrafine ^{222}Rn decay product aerosols have a deposition velocity ~ 100 times that of an attached aerosol. The values of the constant K_2 completely determine the deposition velocity, and were set to give a nominal ultrafine deposition velocity of 0.01 m s^{-1} outdoors.

For the ^{218}Po charge neutralization time, the published data indicate that while a value around 1 s is reasonable, at low ^{222}Rn concentrations in outdoor conditions it could rise to tens of seconds. Alternatively, in wet conditions the value could fall below 1 s. In the diffusion model, the time has been varied between 0.02 and 20 s ($0.05 \leq \lambda_{ch} \leq 50$).

2.2. Experimental methods

2.2.1. *Principles of α -particle track detection in TASTRAK plastic.* The development of TASTRAK plastic for α -particle detection and spectroscopy has been described in a number of previous publications (Fews 1992a,b, Henshaw *et al.* 1994, 1995, 1996).

In the present application, TASTRAK, typically $7 \times 5 \text{ cm}$, is held in air, sampling two categories of aerosol. As described above, ^{222}Rn decay product aerosols on production undergo diffusive dispersion in room air. If during their lifetime they come into contact with a surface, they may adhere to it—a process commonly known as ‘plateout’ but referred to in this paper as (*surface*) *deposition*. A proportion of ^{222}Rn decay product aerosols will therefore deposit

on the TASTRAK surface. On radioactive decay, these aerosols emit α -particles of the characteristic energy of the decay products ^{218}Po and ^{214}Po . Those α -emissions in the direction of the plastic will be recorded at their characteristic full energy of respectively 6.0 and 7.7 MeV and ranges in TASTRAK of 40.2 and 60.5 μm .

The ^{218}Po and ^{214}Po α -particles have respective ranges in air of 5.1 and 7.6 cm. Therefore, a proportion of the ^{222}Rn decay product aerosols in the air in front of the detector as well as ^{222}Rn itself may also be recorded if their α -emissions occur both within range and in the direction of the detector surface. (Note that TASTRAK is not sensitive to the β -particles emitted from the decay products ^{214}Pb and ^{214}Bi , so that the detection of the extremely short half-life ^{214}Po is a signature of these preceding β -emitting decay products.)

In the present work, cone-like etch tracks were revealed by etching in 6.25 M NaOH at 75°C for 4.5 h. The detectors were analysed using an image analysis system in which up to 14 parameters of the shape and size of each recorded α -particle track are measured (Fews 1992a, b). These measurements, combined with track geometry data from calibration exposures, enable the α -particle energies to be directly determined.

Figure 3 illustrates how recorded track size varies with α -particle energy and angle of incidence. The projected track length (the major axis of the etch track opening mouth on steep tracks, and the track length in projection on shallow tracks) is plotted against the minor axis diameter. The data fall within an envelope characteristic of the α -particle track response for the etch conditions employed. Bands are seen which originate from α -emissions from ^{218}Po and ^{214}Po deposited on the plastic surface. These arise from the deposited α -radionuclides observed at constant energy over a range of incident angles. Airborne emission will give a variation of both energy and angle, and discrete bands would not be observed. Therefore, a separate measurement of both the deposited and airborne components is made from the same TASTRAK detector.

2.2.2. *Detection of ^{222}Rn decay product aerosols outdoors.* Use of TASTRAK outdoors requires comparatively long exposure periods to acquire enough counting statistics, although exposures of several days have the advantage of integrating over short-term variations in aerosol concentration. In practice TASTRAK exposed outdoors suffers solar UV damage which limits its exposure period to around 6 days. Under these conditions typical count densities range from a

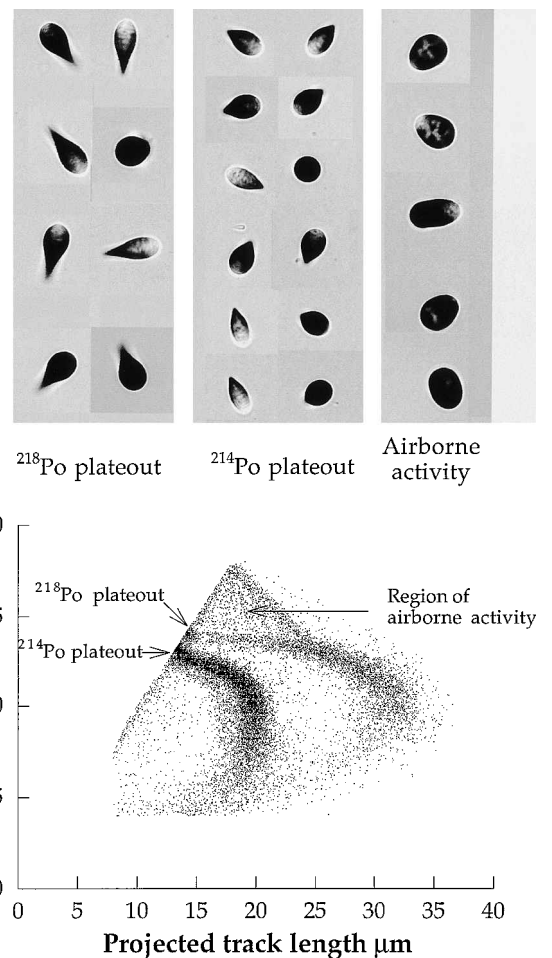


Figure 3. Photomontage of etched tracks and scatter plot of track minor axis versus projected length, showing ^{218}Po and ^{214}Po plateout and the region of airborne activity.

few hundred tracks per cm^2 from deposited activity, to < 30 per cm^2 from the air activity.

Outdoor exposures often result in solid particles landing on the TASTRAK surface. These can introduce microscopic scratches onto the detector surface which when etched grow into defects that can mimic real etch tracks. Such defects are recognized as an extra-Poissonian number of closely separated tracks, taking account of genuine close α -emissions that may be recorded from sequential decays of ^{218}Po and ^{214}Po on the detector surface. Details of this procedure will be described in another publication.

2.2.3. *Layout of detectors under power lines.* Measurements were made at several locations under high voltage transmission lines in south Gloucestershire, UK: (1) 400 kV at OSGB map reference 672830; (2) and (3) 400 kV at two separate locations at OSGB 774775;

(4) 400 kV at OSGB 644838; (5) 275 kV at OSGB 666868; and (6) 132 kV at OSGB 713854.

Two configurations of TASTRAK detectors were employed. One configuration used detectors placed at 30 sampling points 1 m above the ground at right angles to the line. Each sampling point comprised five detectors (the 'pizza box' assembly) mounted on a varnished wooden stake (figure 4a). Three detectors were mounted orthogonally, in the horizontal plane and in parallel and perpendicular planes with respect to the power line; two further detectors were mounted horizontally, looking respectively upwards and downwards. The downwards-facing detector was mounted in the bottom of an inverted plastic pizza box, to protect it from rainfall. In all, including controls, 180 detectors were employed.

This configuration enables the deposition of aerosols to be studied in various directions with respect

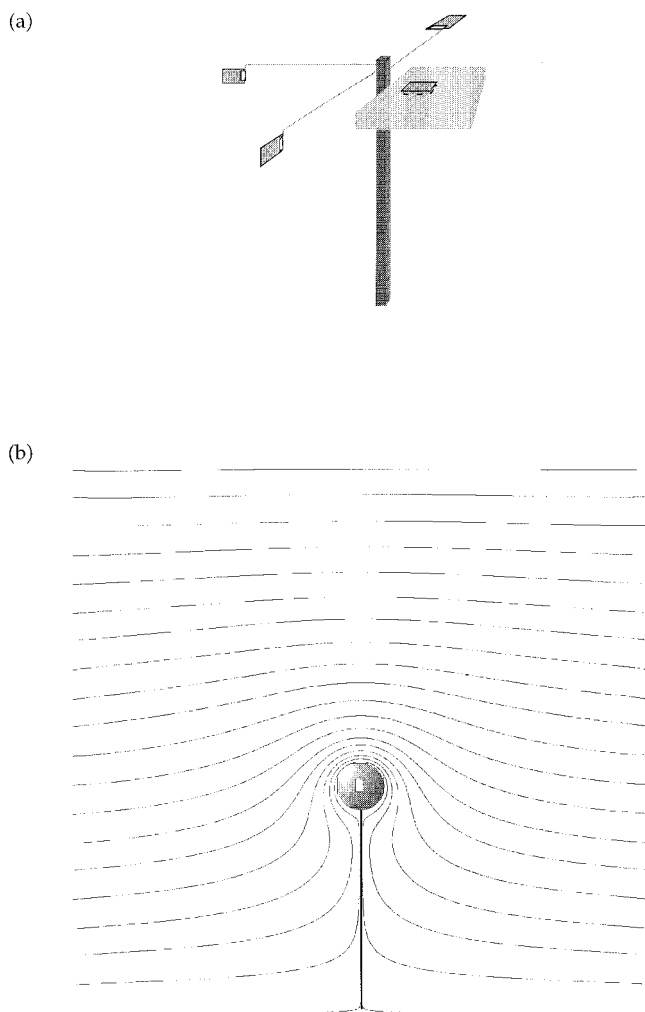


Figure 4. Configuration of TASTRAK detectors under power lines: (a) a perspective view of the pizza box assembly and (b) a sectional view of the sphere assembly showing equipotential contours.

to the power line E-field vector, but suffers a difficulty in that the field distortion around each detecting element is uncertain due to uncertainties in the moisture content of the stake. The E-field distortions around the stake are always uncertain and are likely to be substantial when the stakes are wet. For this reason, and the fact that the detectors are not in the highest field-enhanced region but a few centimetres away from it, the 'pizza box' results are considered to be difficult to interpret.

Therefore another configuration was also employed using a grounded 20 cm diameter metal sphere which created a field perturbation similar to that expected around the human head. Apart from underneath the sphere, field lines would terminate on the sphere at right angles (figure 4b). The sphere was mounted 1 m above the ground with five TASTRAK detectors attached: one horizontally on the top surface and the remainder vertically in north, east, south and west-facing directions. Spheres were placed in the high-field region under the power line and in the low-field region about 100 m away.

Table 1 summarizes the exposures carried out. Weather conditions throughout were recorded. Aerosol concentrations were not measured contemporaneously but background monitoring using a TSI-3010 condensation particle counter found a diurnal variation in the range > 7000 to $< 70\,000\text{ cm}^{-3}$. A typical mean value was $16\,000\text{ cm}^{-3}$.

After each exposure the TASTRAK detectors were processed and measurements were carried out by automated image analysis as described in §2.2.1. These were blind in the sense that the person carrying out the image analysis and subsequent data processing had no knowledge of the position of each TASTRAK detector with respect to the power line.

2.2.4. Calibration. The raw track densities are measured in counts per cm^2 . For a given exposure time they can be expressed in Bq m^{-2} of recorded tracks. The detection efficiency for the deposited activity is calculated using the known track response of TASTRAK, by calculating a cut-off angle. Typical detection efficiencies are 0.268 for ^{218}Po deposition and 0.209 for ^{214}Po depositions.

The airborne activity concentration in Bq m^{-3} is calibrated by simulating emission as a function of height above the TASTRAK surface (the activity concentration is assumed to be uniform with height), and integrating the calculated detection efficiency. This results in an equivalent sampling thickness by the plastic and hence an absolute conversion to activity concentration.

The particle tracks are resolved by energy and therefore a proportion of the airborne activity may

Table 1. Summary of exposure parameters.

Experiment	Location UK grid ref. (OSGB)	Dates	Powerline voltage (kV)	E-field at 1 m height (kV m ⁻¹)	Fraction of time dry	Rain (mm per day)	Average wind speed (m s ⁻¹) ^a
1 ^b	672830	1–9 May 1997	400	4.0	0.86	3.6	3.2
2 ^c	774775	27 Aug–2 Sep 1998	400	3.8	0.97	0.4	1.0
3 ^c	774775	20–26 Jan 1999	400	6.3	0.83	5.3	3.0
4	644838	16–22 Feb 1999	400	7.0	0.86	1.5	3.2
5	666868	5–11 Mar 1999	275	3.4	0.95	0.1	2.6
6	713854	24 Feb–2 Mar 1999	132	1.9	0.25	6.0	5.4

^a 1 m s⁻¹ = 3.6 kilometres per hour = 2.2 miles per hour).

^b Experiment 1 was a ‘pizza box’ run and the others were sphere experiments. ^c Note that the locations of experiments 2 and 3 were not identical.

Sphere exposures were not carried out in experiment 1.

interfere with the deposition bands. For example, an airborne ²¹⁴Po decay of 7.7 MeV may be recorded with a degraded energy of 6.0 MeV, mimicking a 6 MeV ²¹⁸Po deposition. The calibration for the airborne region allows for the presence of the various ²²²Rn-derived species, including those lost into the deposition bands. Simulations suggest that ~5–10% of the airborne tracks are superimposed on each deposition band. Since the ratios of airborne to deposition track densities is ~0.1 for outdoor exposures, then it follows that up to ~0.5–1% of deposition tracks may be wrongly categorized. This will apply nearly equally to ²¹⁸Po and ²¹⁴Po deposition, and therefore the resulting error on both deposition and the ²¹⁴Po/²¹⁸Po ratio is inconsequential. Thoron progeny would reveal additional deposition bands, but were not observed in these experiments. Illustrative track counts on each detector without an E-field are 300–1500 counts for ²¹⁴Po, 100–500 for ²¹⁸Po and 10–50 for the airborne region, where each sphere or pizza box employed five detectors. In general, the errors from counting statistics are negligible compared with the intrinsic variation between adjacent detectors. This intrinsic variation is the basis for the quoted errors in the tables of results. The authors believe this intrinsic variability is generally due to patches of wet deposition, and is worst on the wettest experiments (experiment 6).

3. Results

The model used the standard set of conditions indicated by the constants given in §2.1.2, from which particular parameters were varied.

3.1. Theoretical modelling

Figure 5 shows the variation in ²¹⁸Po-enhanced deposition factor, EF and ²¹⁴Po/²¹⁸Po deposition

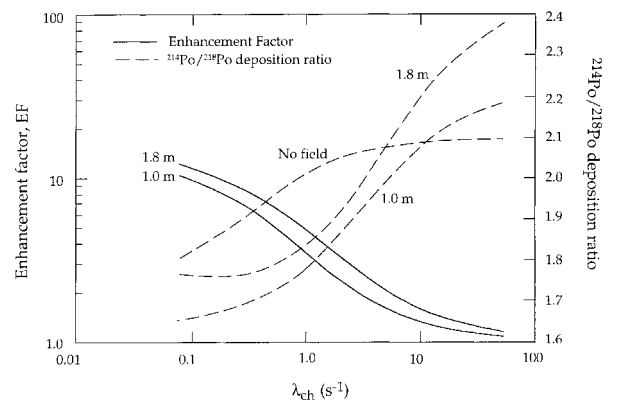


Figure 5. Predicted variation in ²¹⁸Po enhancement factor and ²¹⁴Po/²¹⁸Po deposition ratio in a 5 kV m⁻¹ perturbed AC field as a function of λ_{ch} .

ratio in a 5 kV m⁻¹ perturbed AC field as a function of λ_{ch} . The heights of 1.0 and 1.8 m correspond with a child and adult respectively. The ²¹⁸Po deposition shows an EF of ~4 at $\lambda_{ch} = 1$, increasing to 10–15 for low λ_{ch} (long charged lifetimes). EF values greater than 2 are seen for $\lambda_{ch} \leq 3$ s⁻¹, and therefore significant enhancements are expected for the range of λ_{ch} , which could occur outdoors. The variation in the ²¹⁴Po/²¹⁸Po deposition ratio spans a comparatively small range, between 1.7 and 2. As will be seen later, measured ratios can be larger than this because the ²¹⁴Po deposition is increased due to wet deposition, which is not included in this model. For most values of λ_{ch} the action of the perturbed field is to reduce the ²¹⁴Po/²¹⁸Po deposition ratio, in other words, the enhancements for ²¹⁴Po are somewhat smaller because of a higher proportion of deposition from attached particles.

Figure 6 shows the variation in ²¹⁸Po EF and the ²¹⁴Po/²¹⁸Po deposition ratio with λ_a in a perturbed 5 kV m⁻¹ AC field. The equivalent aerosol concentration is based on an aerosol attachment coefficient of

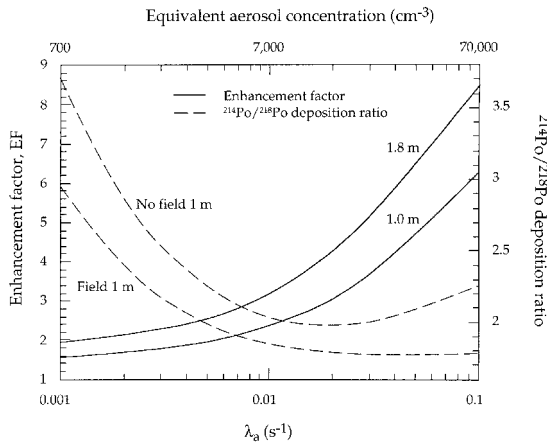


Figure 6. Predicted variation in ^{218}Po enhancement factor and $^{214}\text{Po}/^{218}\text{Po}$ deposition ratio with λ_a and equivalent aerosol concentration in a perturbed 5 kV m^{-1} AC field.

$1.4 \times 10^{-6}\text{ cm}^3\text{ s}^{-1}$ (table 5 in Porstendörfer 1994). The actual aerosol concentrations may differ by a small factor because variations in the attachment coefficient may occur. As indicated in §2.2.3, the range of interest is where $0.01 < \lambda_a < 0.1$, corresponding to an aerosol concentration in the approximate range 7000 to 70 000 cm^{-3} . In this range EF is predicted to lie between 3 and 9 for ^{218}Po .

The form of the variation in the $^{214}\text{Po}/^{218}\text{Po}$ deposition ratio with λ_a and aerosol concentration can be understood qualitatively. In the limit of very low aerosol concentration all ^{222}Rn decay product aerosols are in ultrafine form because there are insufficient aerosols present to allow attachment to larger aerosols. Here (not shown) the deposition ratio is simply equal to the ratio of the mean lifetimes $(^{214}\text{Pb} + ^{214}\text{Bi} + ^{214}\text{Po})/^{218}\text{Po} = 15.2$. Similarly, at very high aerosol concentration (again not shown) it may be considered that all aerosols are in attached form, again giving a deposition ratio of 15.2. In the range of the aerosol concentration of practical interest, where deposition occurs for a combination of ultrafine and attached aerosols, the ratio is less than 15.2 because the ^{218}Po deposition is mainly from ultrafine particles but the ^{214}Po is from a mixture of ultrafine and attached aerosol particles. Therefore the attached deposition of ^{214}Pb and ^{214}Bi is not negligible, and it is this attached deposition that drives the $^{214}\text{Po}/^{218}\text{Po}$ ratio, which is why it can be used as an indicator of aerosol concentration. With no applied field it passes through a minimum of around 2.0 at an attachment rate of around 0.02 to 0.03 s^{-1} , corresponding to a nominal aerosol concentration between 14 000 and 20 000 cm^{-3} . The effect of the perturbed AC field is to decrease the ratio at normal aerosol concentrations because with increas-

ing attachment rate the ultrafine particles spend an increasing proportion of their time in the charged state. As a result the ^{218}Po and ^{214}Po behave more similarly and the effect of neutral ultrafine aerosols is small in this region. This results in the ratio being essentially flat throughout the range of aerosol concentration of interest.

Figure 7 shows the variation in EF and deposition velocity as a function of aerosol size at 1.8 m height with and without a 5 kV m^{-1} perturbed AC field. Increased deposition is seen throughout the aerosol size range up to $10\text{ }\mu\text{m}$. A typical 200 nm aerosol shows an enhanced deposition factor of ~ 2 . The EF values at smaller sizes differ from ^{218}Po ultrafine aerosols in that the particles are assumed to have a Boltzmann charge state, which includes an uncharged component. In the presence of gravity the deposition velocity shows the characteristic minimum in the range 0.2 to $0.3\text{ }\mu\text{m}$ (Porstendörfer 1994). The velocity increase above $0.3\text{ }\mu\text{m}$ is due to the effect of gravitational settling.

Figure 8 shows the variation in ^{218}Po EF with the field-free deposition velocity at 1.8 m height in a perturbed 5 kV m^{-1} AC field and a nominal Earth's DC field of 100 V m^{-1} . Values of $n = 1.5, 2$ and 3 in the turbulent diffusion expression $D_T = K_2 r^n$ have been used. This also yields (not shown) values for the ultrafine/attached deposition ratio of 32, 155 and 756, respectively. Of these, the value for $n = 2$ is within the normal observed range of 100–200 (Porstendörfer 1994). This suggests that $n = 2$, as used by Mayya and Sapra (1997), is appropriate.

Figure 9 shows the variation of EF outdoors and indoors in AC and DC (static) fields. The outdoor and indoor situations were represented by adjusting the constant K_2 to give ultrafine deposition velocities

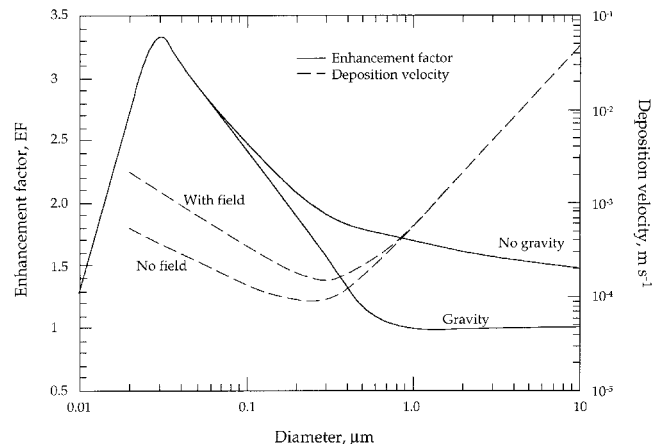


Figure 7. Variation in enhancement factor and deposition velocity as a function of aerosol size with and without a 5 kV m^{-1} perturbed AC field.

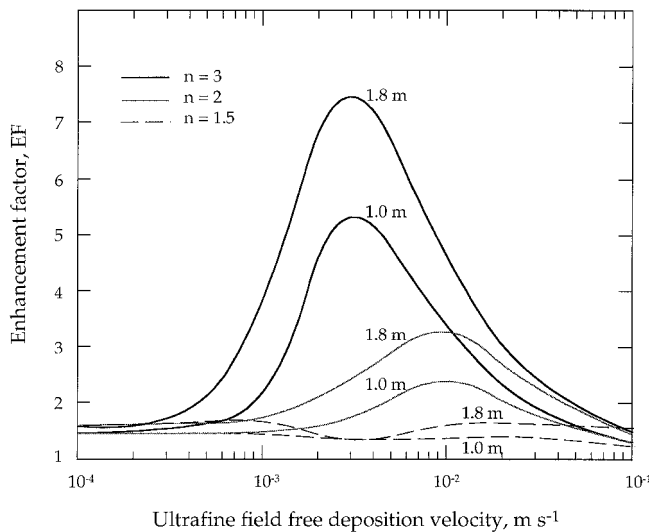


Figure 8. Variation in ^{218}Po enhancement factor with the field-free deposition velocity at 1.0 and 1.8 m heights for $n = 1.5, 2$ and 3 in the turbulent diffusion expression, in a 5 kV m^{-1} perturbed AC field.

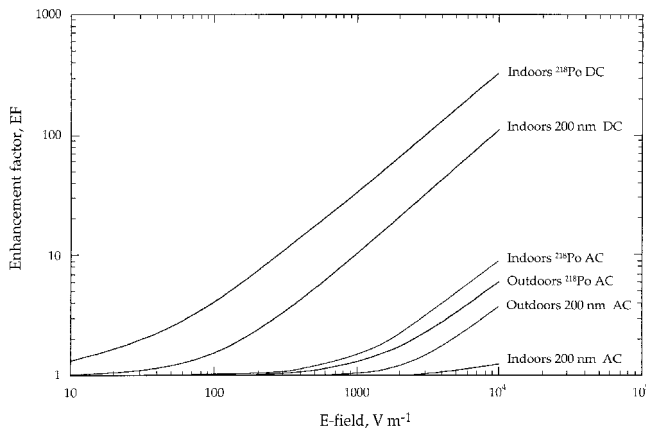


Figure 9. Predicted variation in enhancement factor for ^{218}Po deposition in AC and DC perturbed fields.

in the absence of fields of 0.01 m s^{-1} and 0.0055 m s^{-1} (2 m h^{-1}), respectively. These values are typical of those determined from measurements in the present study and those given by Porstendörfer (1994). Data are shown for the EF in the perturbed field of a 20 cm sphere at a height of 1.8 m, for ^{218}Po and 200 nm aerosol deposition. Enhanced deposition of 200 nm particles is not predicted indoors—this is expected because the deposition boundary layer thickness is much greater than the peak-to-peak oscillation amplitude. Indoors, the effects of turbulent diffusion and wind are depressed as are the effects of the Earth's DC field. Note, however, that EF would rise further for departures from the standard aerosol conditions, i.e. for $\lambda_a > 0.01 \text{ s}^{-1}$ (> 7000 aerosols cm^{-3}) and $\lambda_{ch} < 1 \text{ s}^{-1}$. Significant enhanced depos-

ition is expected indoors for DC fields as low as 10 V m^{-1} for both ^{218}Po and 200 nm particles.

In figure 8, note that since the simulation includes the Earth's DC field, the EF at a deposition velocity of $5.5 \times 10^{-4} \text{ m s}^{-1}$ (the nominal indoor value) is not comparable to the indoor EF value in figure 9 because the AC result here does not include any DC field.

The model calculations were checked by comparing the predictions with known analytical solutions for particular configurations. This test was made using a uniform initial concentration profile in an enclosed system, which has a known analytic solution for the concentration profile as a function of time. The model showed good agreement with the expected concentration profile. The deposition velocity also matched the analytic value ($2/\pi \sqrt{K_2 D_0}$) for the K_2 values used (Mayya and Sapra 1997).

The reliability of the model in predicting the measured data has to be considered because it is a one dimensional representation of an essentially three dimensional air flow and diffusion pattern around the detectors. The model allows particles to flow freely towards the spheres, so depletion in the downwind direction is not modelled. However, the authors are particularly interested in relative deposition, and not the absolute values, and this depends only very weakly on the K_1 and K_2 turbulent diffusion coefficients. The absolute deposition velocity was set at $K_2 = 62 \text{ s}^{-1}$, giving a typical deposition velocity for ultrafine aerosols of 0.01 m s^{-1} , comparable with the deposition velocities measured from the detectors, which were generally in the range $0.005\text{--}0.02 \text{ m s}^{-1}$. The atmospheric profile of ^{222}Rn and its decay products depends on the value of K_1 used, but has no effect on either the deposition velocity to the ground (because this depends on K_2), or on the EF. Therefore, uncertainties in K_1 , and the details of atmospheric transport have a negligible effect on the EF. It is therefore unimportant that transport into the atmosphere can only be an approximation, although it will have some impact on the predicted $^{214}\text{Po}/^{218}\text{Po}$ deposition ratio. Therefore, the model should match the experiment reasonably closely in terms of EF values.

Table 2 gives expected amplitude of oscillation and velocity at deposition for ultrafine aerosols for various field strengths. In the perturbed field at 1.8 m height, values between 2.7 and 27 m s^{-1} or $10\text{--}100 \text{ km h}^{-1}$ are predicted for applied fields between 1 and 10 kV m^{-1} .

3.2. Experimental measurements

Results for the pizza box detectors in experiment 1 are shown in figure 10. Figure 10a shows the

Table 2. Estimated range of amplitude of oscillation of ultrafine aerosol of mobility $1.5 \times 10^{-4} \text{ m}^2 \text{ V}^{-1} \text{ s}^{-1}$ for various 50 Hz field strengths and conditions.

Type of E-field	Applied E-field (kV m^{-1})	E-field at deposition surface (kV m^{-1})	E_{rms} peak-to-peak amplitude from deposition surface (cm)	Particle velocity at surface (m s^{-1})
(a) Unperturbed (uniform field)	1	1	0.14	0.15
	5	5	0.70	0.75
	10	10	1.40	1.5
(b) Perturbed by 20 cm Sphere, at 1 m height	1	10	1.2	1.5
	5	50	4.6	7.5
	10	100	7.4	15
(c) Perturbed by 20 cm Sphere, at 1.8 m height	1	18	2.1	2.7
	5	90	6.9	14
	10	180	10.5	27

measured deposition velocity of ^{218}Po on detectors mounted vertically facing parallel and perpendicular to the line. Note that the deposition velocity shown is for the total ^{218}Po deposition, and is not the ultrafine deposition velocity. The deposition velocity was calculated using the ratio of the deposited activity to the airborne activity, using the standard definition of deposition velocity. For the parallel facing detectors excess deposition is seen within $\pm 25 \text{ m}$ of the line where the E-field exceeds 1.5 kV m^{-1} up to a maximum of 4 kV m^{-1} . No excess deposition is seen in the perpendicular facing detectors, indeed these show an essentially uniform profile of deposition with distance from the line. Figure 10b and c, respectively, show the data plotted as the ratio of deposition in the parallel and perpendicular directions for ^{218}Po and ^{214}Po .

Results for the 20 cm diameter sphere experiments 2 to 6 are shown in figure 11 and table 3. The EF values range from 1.1 to 2.9. The statistical significance was tested using a *t*-test and all values except that at 132 kV were significant at the 95% confidence level. The latter, however, was carried out in particularly adverse weather conditions. Table 1 shows that there was rain 75% of the time for this exposure, indeed this is the only exposure that was predominantly wet. The results from the corresponding pizza box detectors for all of the sphere exposures are given in table 4, where each value is the average of all detector directions.

Table 5 shows a breakdown of the deposition values with respect to direction for experiment 4. The average wind direction was north-westerly. There was remarkable uniformity in the corresponding values on each of the four spheres for both power lines and controls, as indicated by the small spread in each value quoted. The control deposition values are higher on the upwind sides. However, under the

power line, the deposition on the upwind side is particularly enhanced and there is depletion on the downwind side. The observation suggests a coupling of the AC oscillation to turbulent diffusion onto the sphere on the upwind face. The depletion downwind is assumed to be due to the excess upwind deposition. The resulting EF values are higher upwind with an overall excess deposition of 2.86 ± 0.32 and 2.44 ± 0.23 for ^{218}Po and ^{214}Po , respectively.

4. Discussion

4.1. Modelling results

An important feature from figure 9 is the difference in factors governing deposition outdoors compared with indoors. Outdoors, the deposition in power line AC fields is little affected by the Earth's DC field of $\sim 100 \text{ V m}^{-1}$. Apart from field strength, the sensitive parameters are λ_{ch} and λ_a , the latter being sensitive to aerosol size and concentration. As seen in table 2, the velocity of ions at deposition in the perturbed field is in the range $2.7\text{--}27 \text{ m s}^{-1}$ or $10\text{--}100 \text{ km h}^{-1}$, which is faster than typical wind speeds. These velocities underline the nature of the increased exposure on the human head and face. In particular, they will overcome any thermophoretic effects, which have sometimes been invoked to argue against excess deposition of aerosols on the human body.

Indoors, the effects of DC fields are much greater than for AC. The human body can readily pick up static potentials of up to 10 kV in the office and home environment. Under these conditions EF values in excess of 300 are predicted. Such dramatic effects of DC have been proposed as a method of reducing ^{222}Rn decay product concentration indoors (Jonassen 1983). The concern here is with excess deposition on the human body and in this situation even transient

static body potentials could lead to an overall significant excess deposition. Viruses in the relatively small size range of 40–300 nm would be attracted to the body with particular efficiency. The importance of such DC effects indoors are well known and a recent study by Hatch *et al.* (1998) suggested an association between childhood leukaemia and use of TV sets and video games, which might be associated with exposure to static. Future case-control studies of childhood leukaemia in relation to time-varying EMF exposure could usefully be extended to include measurements of exposure to static fields.

The EF predicted for 200 nm aerosols in AC fields is negligible indoors because the particle oscillation amplitude is much smaller than the deposition boundary layer.

The field-free deposition velocity and the form of the turbulent diffusion coefficient were varied to test different turbulence conditions. However, to reproduce a deposition velocity of 0.01 m s^{-1} and an ultrafine/attached deposition velocity ratio of ~ 100 required the use of $D_T = 62.5r^2$. The authors therefore feel this is an appropriate form to represent the conditions experienced on the spheres in outdoor conditions.

4.2. Experimental measurements

The results from the pizza box assembly for experiment 1 demonstrate the principle that excess deposition of aerosols occurs by oscillation along the E-field lines. This is underlined by the fact that no excess deposition was seen on detectors mounted vertically facing a direction perpendicular to the line (figure 10). Uniformity in deposition in this direction was found for both ^{218}Po and ^{214}Po aerosols. This further illustrates that the ^{222}Rn emission from the ground was uniform across the exposure site. This feature is important because small-scale spatial and temporal variations in ^{222}Rn emissions from the ground are known to occur (Robé *et al.* 1992) and if not corrected for could lead to false changes in measured deposition under power lines.

The metal spheres were permanently grounded and therefore the field perturbation was the same

both in all directions and in all weather conditions. The data from table 3 show typical EF values from 1.1 to 2.9. Comparing the values with the prediction

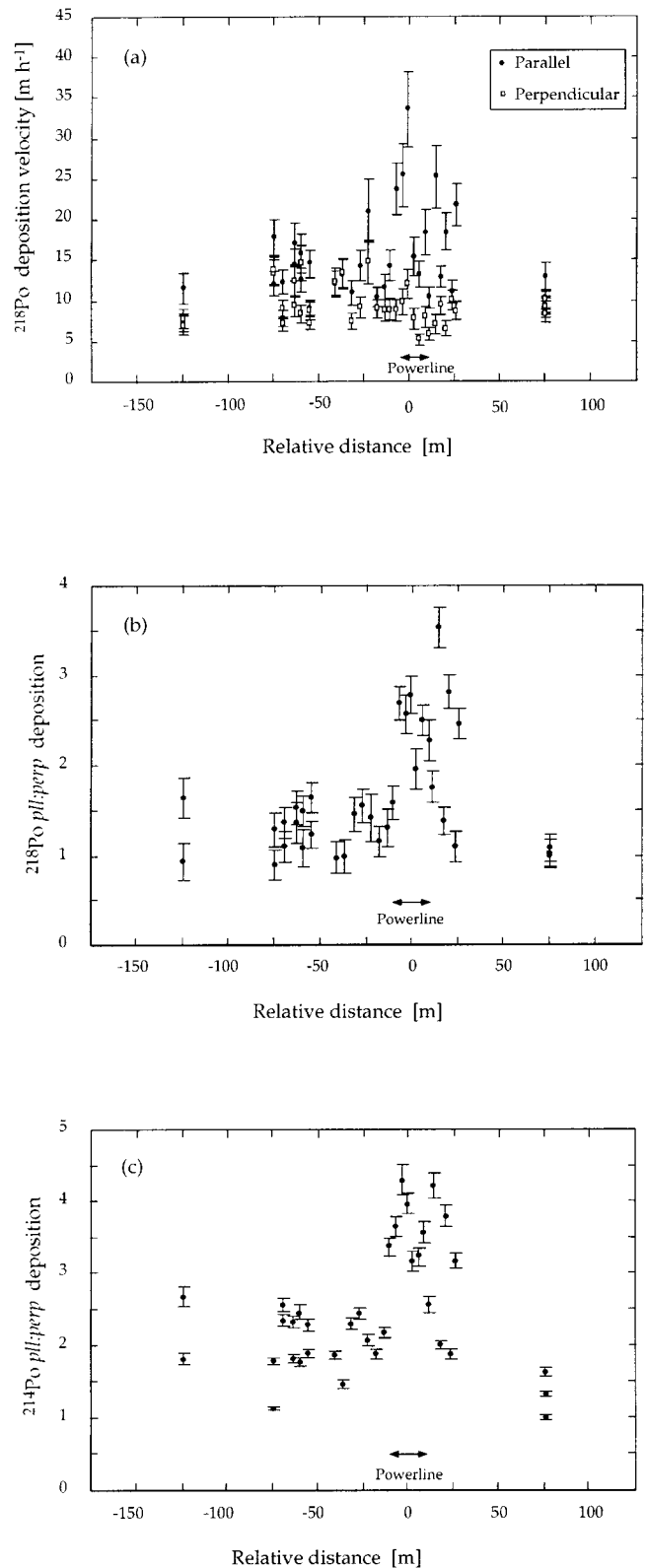


Figure 10. Measured deposition velocity for total deposition (ultrafine and attached particles) for the 'pizza box' detector arrangement shown in figure 4a for the experiment 1 power line exposure. (a) Data points for ^{218}Po deposition on detectors mounted vertically parallel and perpendicular to the line are shown separately. Measured deposition data plotted as the ratio of deposition on detectors mounted parallel versus perpendicular to the line: (b) ^{218}Po deposition versus distance and (c) ^{214}Po deposition versus distance.

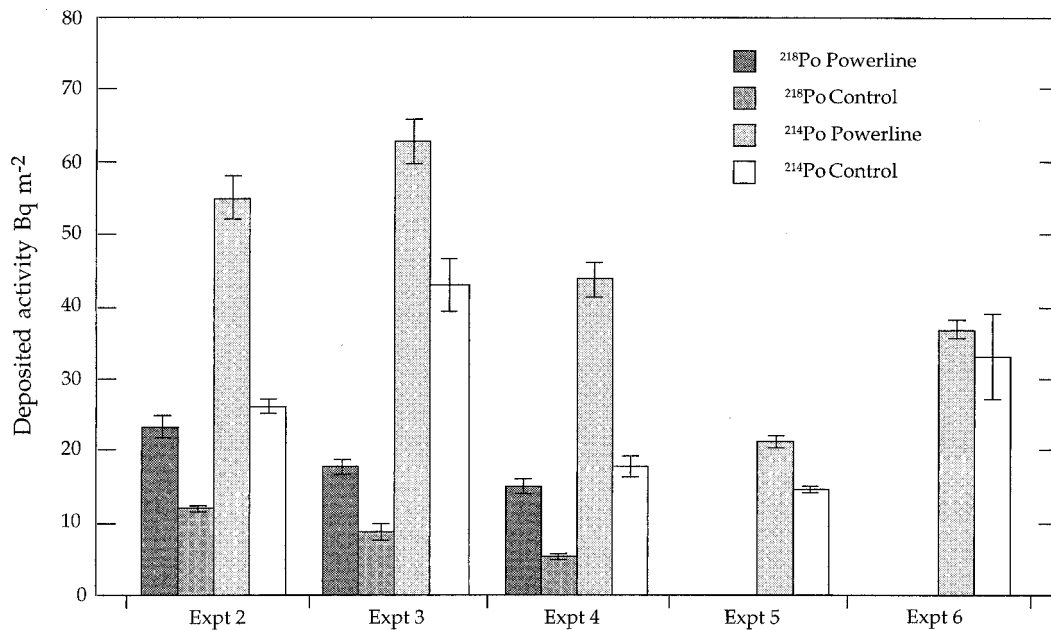


Figure 11. Sphere deposition of ^{218}Po and ^{214}Po aerosols under high voltage power lines and distant controls: experiments 2, 3 and 4, 400 kV; experiment 5, 275 kV and experiment 6, 132 kV.

Table 3. Summary of the sphere results giving the mean enhancement factor under the powerline.

Experiment	No of spheres expt, controls	^{218}Po			^{214}Po		
		Powerline Bq m^{-2}	Control Bq m^{-2}	Enhancement factor	Powerline Bq m^{-2}	Control Bq m^{-2}	Enhancement factor
2	2, 2	23.32 ± 1.57	11.92 ± 0.42	1.96 ± 0.15 (0.042)	54.96 ± 2.89	26.15 ± 1.10	2.10 ± 0.14 (0.033)
3	4, 4	17.80 ± 0.99	8.91 ± 1.12	2.00 ± 0.27 (0.001)	62.90 ± 3.12	43.05 ± 3.61	1.46 ± 0.14 (0.019)
4	4, 4	15.07 ± 0.97	5.27 ± 0.48	2.86 ± 0.32 ($< 10^{-4}$)	43.70 ± 2.29	17.92 ± 1.44	2.44 ± 0.23 ($< 10^{-4}$)
5	2, 2	-	-	-	21.10 ± 0.83	14.76 ± 0.40	1.43 ± 0.07 (0.028)
6	2, 2	-	-	-	36.90 ± 1.26	33.10 ± 5.99	1.11 ± 0.21 (0.39)*

*Not significant.

p -value given in brackets.

in figure 9 suggests that λ_{ch} is likely to be in the region $1-2 \text{ s}^{-1}$, giving a neutralization time somewhat less than 1 s. In these conditions, enhancement is expected on the spheres but not on the pizza boxes with an unperturbed field.

4.3. General aerosol behaviour

Significant enhanced body deposition in the region 1.5–2.0 is expected for general aerosol particles in the entire size range 10 nm to 10 μm , as shown in figure 7. This result is entirely independent of radon decay product behaviour, although experimental data for this enhancement is not available. For a

given aerosol size spectrum, the theoretical prediction could be used to estimate the increased mass deposition of pollutant aerosols under power lines. This could include the expected increased deposition of viruses and bacteria in air. It should also be noted that detectable excess deposition on the head would be expected for all common transmission line voltages. This is borne out in the measurements at 400 and 275 kV. The EF value at 132 kV in the current measurements was not statistically significant, although as stated above, the measurements were carried out in particularly wet and windy conditions.

The existence of meaningful excess deposition in terms of exposure to non- ^{222}Rn pollutants is essen-

Table 4. Summary of pizza box total deposition values in Bq m^{-2} for sphere exposures.

Exposure	Powerline		Control	
	^{218}Po	^{214}Po	^{218}Po	^{214}Po
2	7.6 ± 0.3 (15)	16.9 ± 0.7 (15)	8.2 ± 1.2 (3)	17.6 ± 3.4 (3)
3	7.9 ± 0.5 (14)	34.9 ± 1.6 (14)	7.8 ± 0.5 (12)	27.3 ± 1.7 (12)
4	3.92 ± 0.19 (1)	13.9 ± 0.4 (1)	3.10 ± 0.40 (2)	14.2 ± 1.3 (2)
5	–	12.7 ± 0.3 (1)	–	10.7 ± 0.3 (1)
6	–	17.9 ± 0.4 (1)	–	21.2 ± 0.4 (1)

Standard errors are shown. Number of detectors is given in brackets; where only one detector is available the error is based on the counting statistics.

Table 5. Directionality of ^{218}Po -enhanced deposition around the spheres for experiment 4.

Direction	^{218}Po powerline	^{218}Po control	EF
Top	16.20 ± 1.81	6.73 ± 0.71	2.41 ± 0.37
North-west	31.35 ± 0.57	6.00 ± 0.32	5.23 ± 0.29
South-east	1.80 ± 0.43	3.30 ± 0.16	0.55 ± 0.13
North-east	3.35 ± 0.58	4.10 ± 0.58	0.82 ± 0.18
South-west	22.65 ± 1.35	6.23 ± 0.70	3.64 ± 0.46

tially due to the perturbation of the E-field by the human body. In particular, no detectable effect is expected in the unperturbed field. This is in broad agreement with the overall pizza box results in table 4 and suggests that the increased deposition on pizza box assemblies in figure 10 (experiment 1) may indeed be attributed to uncertain field enhancement around individual detectors due to the wet conditions.

The deposition model suggests that the aerosol oscillation mechanism, coupled to turbulent diffusion, does not affect the air concentration of aerosols. Miles and Algar (1997) used air sampling to measure ^{222}Rn decay product activity in air and found no difference in values near compared with away from a 400 kV power line. McLaughlin and Gath (1999) also found no difference in ^{222}Rn decay product activity either in air or on surfaces near compared with away from a 400 kV power line. Their results, however, appear to be based on only four data points in the unperturbed field. Also, there is no indication that the detectors were aligned at right angles to the power line E-field vector. In any case, both these results and those of Miles and Algar (1996) are entirely consistent with the modelling presented here, which predicts that neither the airborne activity nor

the deposition in the *unperturbed* field will show any enhancement under power lines.

4.4. Implications for dose

The observed increased deposition on spheres representing the human head under high voltage power lines is in good agreement with the theoretical model which demonstrates a mode of increased exposure to ^{222}Rn marker aerosols under high voltage power lines. The model suggests that aerosols in general, including viruses and bacteria, will be subject to increased deposition and this could be tested experimentally in further work.

There is current interest in the radiation dose to the basal layer from ^{218}Po and ^{214}Po deposition on the skin and possible links with skin cancer. For indoor exposure at the average UK ^{222}Rn concentration of 20 Bq m^{-3} the annual equivalent dose to the skin basal layer on the face and neck has been estimated as 2.5 mSv y^{-1} (range $1.7\text{--}17 \text{ mSv y}^{-1}$) (Eatough 1997). Outdoors, the deposition velocity is ~ 20 times greater than indoors so that even accounting for lower ^{222}Rn concentration outdoors, the dose conversion per unit time is much greater outdoors than indoors.

It is possible to estimate the indoor and outdoor doses from the authors' own experimental measurements, assuming that deposition occurs at a constant rate throughout the experiments. Indoors, the unpublished measurements give average respective ^{218}Po and ^{214}Po deposition rates of 1.03 and 2.18 Bq m^{-2} at 20 Bq m^{-3} . This is consistent with results from modelling using a deposition velocity of $5 \times 10^{-4} \text{ m s}^{-1}$, similar to that reported by Porstendörfer (1994). Using equivalent dose conversion factors for the face of 0.7 and $1.1 \mu\text{Sv y}^{-1}$ per decay per cm^2 for ^{218}Po and ^{214}Po respectively, estimated by Eatough (1997), this yields a dose rate of 9.8 mSv y^{-1} . By comparison, the deposition rates outdoors away from power lines reported above are 7.5 Bq m^{-2} for ^{218}Po and 22.6 Bq m^{-2} for ^{214}Po . These values are consistent with an outdoor ^{222}Rn concentration of 7 Bq m^{-3} and an ultrafine deposition velocity of 0.01 m s^{-1} . This deposited activity corresponds to a dose rate of 95 mSv y^{-1} for continuous exposure outdoors.

If a person spends 10% of the time outdoors then half a person's skin dose arises outdoors, and typical skin doses are twice those arising from indoor exposure alone. Using these figures, the total dose rate (outdoors + indoors) away from power lines is 18.3 mSv y^{-1} . This mean value is consistent with recently reported values found on personal skin dosimeters (Eatough *et al.* 1999). Under power lines,

however, measurements suggest that the outdoor dose is increased in the range 1.4–2.9 so that the total skin dose rate becomes 22.1–36.4 mSv y^{-1} , an increase in total exposure in the range 1.2–2.0. These surprising results have consequences for the skin cancer risk associated with natural ^{222}Rn exposure, especially for those living under high voltage power lines.

Quantitative estimates of dose to internal organs are difficult to make from the present work. Table 2 suggests that the velocity at deposition of ultrafine aerosols onto the human head is around 14 m s $^{-1}$ (50 km h $^{-1}$) in an AC field of 5 kV m $^{-1}$. Aerosols landing near the nose and mouth might deposit with even higher velocities owing to the higher field distortion in these regions where they might be susceptible to increased inhalation. In the case of some chemical species, there may be the possibility of increased absorption through the skin.

Further mechanisms of increased exposure to aerosols near power lines are under investigation. The authors are particularly interested in the effect of corona losses, which lead to the emission of large fluxes of ions into the atmosphere. The resulting atmospheric space charge can reverse the direction of the Earth's natural DC field up to several hundred metres from the line. In some circumstances, corona ions will have the effect of increasing the steady state charge on aerosols near power lines, which in turn will increase their lung deposition probability on inhalation (Cohen *et al.* 1998). This subject will be discussed in a separate paper.

4.5. Links with childhood leukaemia and traffic density

The authors suggest the results presented here are relevant to the reported epidemiological associations between high voltage power lines and childhood and adult leukaemia, given that it is only one of several mechanisms of increased exposure to pollutants near power lines. The body of evidence relating traffic pollution with childhood leukaemia is such that as a working hypothesis the link can be considered causal. The authors point out again that this link concerns exposure outdoors as does the increased exposure near power lines. Some studies have shown increased incidence of lung cancer in relation to power line exposures (Erren 1996, Henshaw 1997). Given that environmental pollution contains polycyclic aromatic hydrocarbons, including known lung carcinogens such as benzo[α]pyrene, it may be assumed that there is increased exposure to these agents under power lines.

5. Summary

1. Taking into account the special features of ^{222}Rn decay product aerosols, notably their initial positive charge state and ultrafine form, such aerosols are a useful marker of general aerosol behaviour in AC fields outdoors near high voltage power lines.
2. A theoretical model predicts enhanced aerosol deposition on the human head in typical power line fields.
3. Repeated measurements under high voltage power lines of ^{222}Rn decay product aerosol deposition on spheres mimicking the human head show EF values in the range 1.4–2.9 in a variety of weather conditions, in good agreement with the theoretical model.
4. The results suggest that the total (indoor + outdoor) dose to the basal layer of facial skin from deposited ^{218}Po and ^{214}Po is increased by between 1.2 and 2.0 for 10% of time spent outdoors under high voltage power lines.
5. The model suggests that, outdoors, the aerosol deposition in AC fields is only weakly affected by the Earth's natural DC field, but indoors the effects of DC (static) fields are likely to be significantly greater than for AC fields.
6. Overall, the present results lend support to the working hypothesis that the associations between childhood cancer and power (transmission) lines are causal and are due to increased exposure to environmental pollutants near power lines, notably from vehicle exhausts.

It is hoped that the findings in this paper will be of value in designing future case-control studies of childhood leukaemia and other cancers in relation to high voltage power (transmission) line exposures, as well as re-assessing the results of existing studies. The overall aim in future work is to establish risk factors for living under power lines based on increased exposure to environmental pollution.

Acknowledgements

The authors thank Nicola Holden and Adrian Castelino-Prabhu for assistance in detector assembly. This work was supported by the UK Medical Research Council, the Department of Health, the Foundation for Children with Leukaemia and the Spandex Foundation, UK.

References

- AHLBOM, A., FEYCHTING, M., KOSKENVUO, M., OLSEN, J. H., PUKKALA, E., SCHULGEN, G. and VERKASALO, P., 1993,

- Electromagnetic fields and childhood cancer. *Lancet*, **342**, 1295–1296.
- CHENG, Y. S., SU, Y. F., NEWTON, G. J. and YEH, H. C., 1992, Use of a graded diffusion battery in measuring the activity size distributions of thoron progeny. *Journal of Aerosol Science*, **23**, 361–372.
- CLEMENT, C. F. and HARRISON, R. G., 1992, The charging of radioactive aerosols. *Journal of Aerosol Science*, **23**, 481–504.
- COHEN, B. S., XIONG, J. Q., FANG, C. P. and LI, W., 1998, Deposition of charged particles on lung airways. *Health Physics*, **74**, 554–560.
- CRUMP, J. G. and SEINFELD, J. H., 1981, Turbulent deposition and gravitational sedimentation of an aerosol in a vessel of arbitrary shape. *Journal of Aerosol Science*, **12**, 405–415.
- EATOUGH, J. P., 1997, Alpha-particle dosimetry for the basal layer of the skin and the radon progeny ^{218}Po and ^{214}Po . *Physics in Medicine and Biology*, **42**, 1899–1911.
- EATOUGH, J. P., WORLEY, A. and MOSS, G. R., 1999, Personal monitoring of ^{218}Po and ^{214}Po radionuclide deposition onto individuals under normal environmental exposure conditions. *Physics in Medicine and Biology*, **44**, 2227–2239.
- ERREN, T. C., 1996, Re: Association between exposure to pulsed electromagnetic fields and cancer in electric utility workers in Quebec, Canada, and France. *American Journal of Epidemiology*, **143**, 841.
- FEWS, A. P., 1992a, Fully automated image analysis of etched tracks. *Nuclear Instruments and Methods in Physics Research*, **B72**, 465–478.
- FEWS, A. P., 1992b, Flexible analysis of etched nuclear particle tracks. *Nuclear Instruments and Methods in Physics Research*, **B72**, 91–103.
- FEYCHTING, M. and AHLBOM, A., 1993, Magnetic fields and cancer in children residing near Swedish high-voltage power lines. *American Journal of Epidemiology*, **138**, 467–481.
- HATCH, E. E., LINET, M. S., KLEINERMAN, R. A., TARONE, R. E., SEVERSON, R. K., HARTSOCK, C. T., HAINES, C., KAUNE, W. T., FRIEDMAN, D., ROBISON, L. L. and WACHOLDER, S., 1998, Association between childhood acute lymphoblastic leukaemia and use of electrical appliances during pregnancy and childhood. *Epidemiology*, **9**, 234–245.
- HENSHAW, D. L., 1997, Electromagnetic field exposure and lung cancer. *American Journal of Epidemiology*, **146**, 366.
- HENSHAW, D. L., ALLEN, J. E., KEITCH, P. A. and RANDLE, P. H., 1994, The spatial distribution of naturally occurring ^{210}Po and ^{226}Ra in children's teeth. *International Journal of Radiation Biology*, **66**, 815–826.
- HENSHAW, D. L., KEITCH, P. A. and JAMES, P. R., 1995, Lead-210, polonium-210 and vehicle exhaust pollution. *Lancet*, **345**, 324–325.
- HENSHAW, D. L., ROSS, A. N., FEWS, A. P. and PREECE, A. W., 1996, Enhanced deposition of radon daughter nuclei in the vicinity of power frequency electromagnetic fields. *International Journal of Radiation Biology*, **69**, 25–38.
- HINDS, W. C., 1982, *Aerosol Technology—Properties, Behaviour and Measurement of Airborne Particles* (New York: John Wiley & Sons).
- HOPKE, P. K., 1989, Use of electrostatic collection of ^{218}Po for measuring Rn. *Health Physics*, **57**, 39–42.
- HOWARD, A. J. and STRANGE, W. P., 1992, Measurement of $^{218}\text{Po}^+$ neutralisation rates in gases. *Nuclear Instruments and Methods in Physics Research*, **A311**, 378–385.
- INTERNATIONAL COMMISSION ON NON-IONISING RADIATION PROTECTION (ICNIRP), 1998, Guidelines for limiting exposure to time varying electric, magnetic and electromagnetic fields (up to 300 GHz). *Health Physics*, **74**, 494–512.
- JACOBI, W., 1972, Activity and potential α -energy of ^{222}Rn and ^{222}Rn daughters in different air atmospheres. *Health Physics*, **22**, 441–450.
- JACOBI, W. and ANDRÉ, K., 1963, The vertical distribution of radon-222 and radon-220 and their decay products in the atmosphere. *Journal of Geophysical Research*, **68**, 3799–3814.
- JONASSEN, N., 1983, The effect of electric fields on ^{222}Rn daughter products in indoor air. *Health Physics*, **45**, 487–491.
- LINDQUIST, R., NILSSON, B., EKLUND, G. and GAHRTON, G., 1991, Acute leukaemia in professional drivers exposed to gasoline and diesel. *European Journal of Haematology*, **47**, 98–103.
- MAYYA, Y. S. and SAPRA, B. K., 1997, Radon daughter deposition on surfaces carrying alternating electric fields. *International Journal of Radiation Biology*, **71**, 69–74.
- MCLAUGHLIN, J. P. and GATH, G., 1999, Radon progeny activities in the vicinity of high voltage power lines. *Radiation Protection Dosimetry*, **4**, 257–262.
- MERCER, T. T., 1976, The effect of particle size on the escape of recoiling RaB atoms from particulate surfaces. *Health Physics*, **31**, 175–176.
- MILES, J. C. H. and ALGAR, R. A., 1997, Measurements of radon decay product concentrations under power lines. *Radiation Protection Dosimetry*, **74**, 193–194.
- NATIONAL INSTITUTE OF ENVIRONMENTAL HEALTH SCIENCES, 1998, Working Group Report: Assessment of health effects from exposure to power-line frequency electric and magnetic fields, edited by C. J. Portier and M. S. Wolfe. US DoE/NIEHS/NIH (Research Triangle Park: NIEHS).
- NATIONAL INSTITUTE OF ENVIRONMENTAL HEALTH SCIENCES, 1999, NIEHS Report on health effects from exposure to power-line frequency electric and magnetic fields. NIH Publication No. 99-4493 (Research Triangle Park: NIEHS).
- NATIONAL RADIOLOGICAL PROTECTION BOARD (NRPB), 1994, Supplementary report by the advisory group on non-ionising radiation, of 12 April 1994, Chairman: Sir Richard Doll. *Radiological Protection Bulletin*, No. 154, June 1994.
- NORLINDER, R. and JÄRVHOLM, B., 1997, Environmental exposure to gasoline and leukaemia in children and young adults—an ecological study. *International Archives of Occupational and Environmental Health*, **70**, 57–60.
- OLSEN, J. H., NIELSEN, A. and SCHULGEN, O., 1993, Residence near high-voltage facilities and risk of cancer in children. *British Medical Journal*, **307**, 891–895.
- PORSTENDÖRFER, J., 1984, Behaviour of radon daughter products in indoor air. *Radiation Protection Dosimetry*, **7**, 107–113.
- PORSTENDÖRFER, J., 1994, Properties and behaviour of radon and thoron and their decay products in the air. *Journal of Aerosol Science*, **25**, 219–263.
- RAES, F., 1985, Description of the properties of unattached ^{218}Po and ^{212}Pb particles by means of the classical theory of cluster formation. *Health Physics*, **49**, 1177–1187.
- ROBÉ, M. C., RANNOU, A. and LE BRONEC, J., 1992, Radon measurement in the environment in France. *Radiation Protection Dosimetry*, **45**, 455–457.
- ROBINSON, A. A., 1991, Cancer deaths due to all causes, its relationship with vehicle travel in Australia, Japan and European Countries. *Medical Hypotheses*, **36**, 166–171.
- SAVITZ, D. A. and FEINGOLD, L., 1989, Association of childhood cancer with residential traffic density. *Scandinavian Journal of Work, Environmental Health*, **15**, 360–363.

- SEHMEL, G. A., 1973, Particle eddy diffusivities and deposition velocities for isothermal flow and smooth surfaces. *Journal of Aerosol Science*, **4**, 125–138.
- SHI, B. and HOPKE, P. K., 1991, Study of neutralisation of ^{218}Po by small recombination in O_2 , Ar and N_2 . *Health Physics*, **61**, 209–214.
- TYNDALL, A. M., 1938, *The Mobility of Positive Ions in Gases* (Cambridge, UK: Cambridge University Press).
- VERKASALO, P. K., PUKKAL, E., HONGISTO, M. Y., VALJUS, J. E., JÄRVINDEN, P. J., HEIKKILÄ, K. V. and KOSKENVUO, M., 1993, Risk of cancer in Finnish children living close to power lines. *British Medical Journal*, **307**, 895–899.